Additive manufacturing of thin-walled SS316L-IN718 functionally graded materials by direct laser metal deposition

Ghanavati, R., Naffakh-Moosavy, H. & Moradi, M.

DOI 10.1016/j.jmrt.2021.09.061
ESSN 2238-7854

Publisher: Elsevier

JOURNAL OF MATERIALS RESEARCH AND TECHNOLOGY 2021;15:2673–2685

Available online at www.sciencedirect.com

jmr&t Journal of Materials Research and Technology

journal homepage: www.elsevier.com/locate/jmrt

Original Article

Additive manufacturing of thin-walled SS316L-IN718 functionally graded materials by direct laser metal deposition

Reza Ghanavati [a], *Homam Naffakh-Moosavy* [a,*], *Mahmoud Moradi* [b]

[a] *Department of Materials Engineering, Tarbiat Modares University (TMU), PO Box 14115-143, Tehran, Iran*
[b] *School of Mechanical, Aerospace and Automotive Engineering, Faculty of Engineering, Environment and Computing, Coventry University, Gulson Road, Coventry, CV1 2JH, UK*

ARTICLE INFO

Article history:
Received 22 August 2021
Accepted 16 September 2021
Available online 24 September 2021

Keywords:
Additive manufacturing
Thin-walled
Functionally graded materials
Laser deposition
Microstructure

ABSTRACT

Functionally graded materials (FGMs) are a good response to those advanced applications that service requirements are diverse and require high performance. Additive manufacturing (AM) technology, with its many advantages, including high flexibility for complex geometries and near-net-shape integration, has attracted special attention in the development of FGMs. In this research, the solidification behavior and microstructure evolution in the laser additive manufacturing of thin-walled stainless steel 316L-Inconel 718 graded materials have been studied with the help of solidification concepts in the welding metallurgy, according to the common principles of welding and additive manufacturing processes. For this purpose, optical and electron microscopy techniques, X-ray energy dispersive spectroscopy, and microhardness measurement were used along the build direction of FGMs with different transition designs. Microstructure evaluation showed that due to re-melting of layers, despite the increased undercooling in the build direction, morphological evolution occasionally occurred periodically between solidification modes, and due to thermal accumulation, a coarser microstructure is formed in the final layers. In addition, in the chemical analysis, it was observed that the mixing of adjacent layers caused by dilution led to a deviation of the composition distribution from the desired design. Also, the microsegregation of some elements during the non-equilibrium solidification of the process caused secondary phases such as carbides and intermetallic compound of Laves, which can have an adverse effect on the mechanical properties of the structure. However, microhardness variations along the cross-section of the samples showed that the gradation of the dissimilar thin-walled structure can effectively bring the properties and behavior of adjacent layers closer together and therefore be very useful in improving the service life.

* Corresponding author.
E-mail address: h.naffakh-moosavy@modares.ac.ir (H. Naffakh-Moosavy).

https://doi.org/10.1016/j.jmrt.2021.09.061

1. Introduction

The development of industries and the subsequent emergence of new issues and needs related to improving productivity have made materials selection ever-critical and influential, besides other requirements. Looking from the past to the present can be understood; materials tailored to the needs of each period have been discovered one after another, and after a flourishing time, have found a position commensurate with newer and alternative materials. So that in the present era, there are few cases in advanced applications where only one material can meet all the requirements of service conditions, and often designers have to use different materials together [1]. Although dissimilar joints or composites are commonly considered major candidates for multifunctional applications, their numerous weaknesses, mainly due to the sharp interface, can lead to premature and even sudden structure failure [1,2]. In contrast, functionally graded materials (FGMs) as a group of advanced engineering materials, with the benefit of a smooth change in properties and behavior in one or more preferential directions, due to the gradual change of chemical composition or microstructure, can effectively improve the performance and service life of multi-material structures [3].

Chemical/physical vapor deposition (CVD/PVD), thermal spraying, powder metallurgy, centrifugal casting, and self-propagating high temperature synthesis (SHS) are among the most common fabrication methods of FGMs [4]. However, these methods face serious problems in the development of FGMs due to limitations of the geometry and density of the parts produced, high energy consumption, and environmental pollution [5]. In recent years, additive manufacturing (AM) technology has attracted much attention to FGMs fabrication due to its nature, i.e., adding materials preferably layer-by-layer to achieve the final shape. Accordingly, it can eliminate many disadvantages of the conventional manufacturing methods. In addition, AM brings important advantages, such as high flexibility in the production of complex and integrated parts and customization (on-demand production) [6,7]. On the other hand, it seems that due to the rapid development in high performance metals and alloys, AM [8] has caused double attention in using this technology to fabricate metallic FGMs [9,10].

In the meantime, the combination of properties such as high strength and excellent high-temperature corrosion resistance in nickel-based superalloys, and properties such as good corrosion resistance, lower cost and weight in stainless steels, makes the tendency to use these two alloys together in important industries such as power plant, nuclear, aerospace, and oil refining [11]. Although the common techniques for applying these two classes of alloys together are often fusion welding, the poor resistance of the weld to liquation cracking [12] has led to various alternatives techniques including gradient additive manufacturing. For example, Lin et al. [13] studied laser rapid forming (LRF) of SS316L/Rene88DT graded material. Shah et al. [14] investigated the effect of key parameters of the laser direct metal deposition process (laser power and powder flow rate) on the microstructure and mechanical properties of SS316L/IN718 graded structure. Savitha et al. [15], in a study on additively manufactured dual materials from SS316 and IN625, demonstrated that regardless of whether a discrete or gradient interface is designed, the change in chemical composition near the interface due to dilution is gradual, and the yield strength is always comparable to the weaker component, i.e., SS316. However, Zhang et al. [16] stated in a similar study that the yield strength of graded samples is similar to that of IN625, and the tensile strength is close to SS316L. In another study by Carroll et al. [17], thermodynamic modeling by the CALculation of PHAse Diagrams (CALPHAD) method along with experimental evaluation were used to determine the role of metal monocarbides in the form (Mo, Nb)C as responsible for cracking in the graded structure of SS304L and IN625 fabricated by directed energy deposition (DED). The effect of gradation steps (5%, 10%, and 20%) in laser additive manufacturing SS316L/IN718 FGM on the microstructure and mechanical properties was studied by Su et al. [18]. They reported that the best combination of tensile properties, with tensile strength of 527.05 MPa and 26.21% elongation, was obtained for the FGM by 10% chemical increments.

Also, as known, using high performance engineering materials for industrial applications (like parts in power plant and land based and aero based gas turbines) is inevitable. These materials should be tough, strong and affordable. Stainless steels, especially SS316, are interesting materials for these purposes. To improve the durability, high temperature corrosion resistance and strength of SS316, more efficient and expensive materials (such as superalloys especially Inconel 718) should be used as covering materials. This combination of properties and economical consideration in SS316 and IN718 can make their FGMs produced by additive manufacturing an attractive candidate for research and industrialization [14,16]. It should be noted that using parts entirely produced from IN718 is very expensive, and also, using SS316 alone cannot guarantee the appropriate properties for such applications. Accordingly, AM of SS316-IN718 FGMs can promote economical, technological and commercial benefits and developments.

Despite valuable findings in previous research, it seems that the analysis of solidification behavior and microstructure evolution in the additively manufactured gradient structures of stainless steels-nickel base superalloys has received less attention. Therefore, in the present work, due to the salient similarities between the welding and additive manufacturing processes [19,20], the principles and concepts of solidification previously developed in welding metallurgy have been used. These principles are utilized to describe the macrostructure and microstructure, chemical and phase composition, and their relationship to the microhardness distribution along the build direction of stainless steel 316L-Inconel 718 functionally graded materials by AM process.

2. Materials and methods

Gas-atomized powders of low carbon stainless steel 316 (SS316L) and Inconel 718 (IN718) nickel-based superalloy, respectively with an average diameter of 110 and 70 microns (Fig. 1), and the nominal chemical compositions presented in

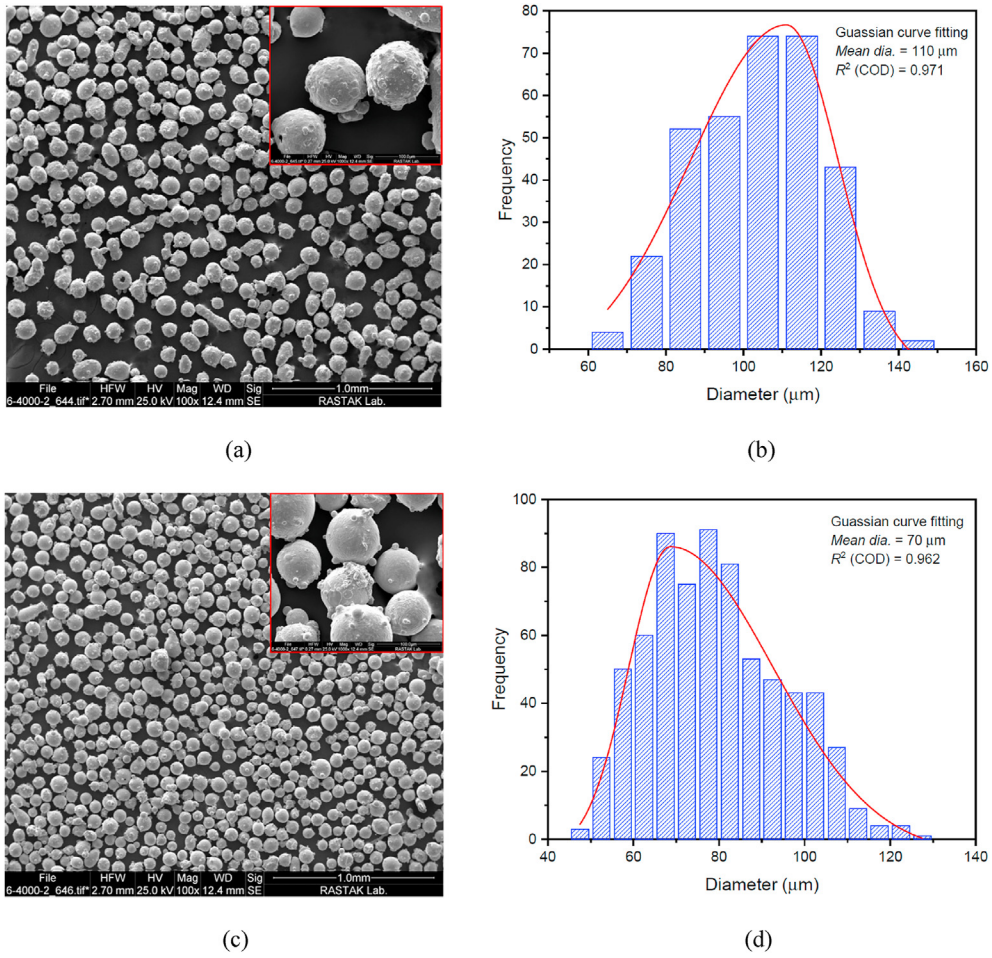

Fig. 1 – SEM image of (a) SS316L and (c) IN718 powder; Particle size distribution of (b) SS316L and (d) IN718.

Table 1, were used to fabricate dissimilar and gradient structures on an SS316L substrate with dimensions of 5 5 1 cm. Before the process, the surface of the substrate was first washed by a water/soap mixture, and then cleaned with alcohol (96% purity). Three thin-walled samples, each consisting of six layers, as shown in Fig. 2a, were designed to compare better and understand the gradient effect. As can be seen, sample 1 has no gradient transition between 3 layers SS316L and 3 layers IN718; sample 2 consists of 2 layers with an equal weight percentage of base alloys between 2 layers SS316L and 2 layers IN718; and sample 3 with substitutional steps of 20 wt.% IN718 instead of SS316L were considered between the first and last pure layers. Direct laser metal deposition (DLMD) additive manufacturing system, equipped with 1 kW continuous-wave fiber laser (model YFL-1000) of wavelength 1080 nm, four-channel brass nozzle to deliver powders coaxial with the laser beam, powder feeder with two separate containers, carrier and shielding argon gas, and CNC table was used to fabricate the samples. Before starting the process, SS316L and IN718 powders are poured separately into the feeder containers, and during the process by independently adjusting the rotation speed of the powder feeder discs (as presented in Table 2), the weight percentage required of each alloy to deposit each layer according to the designs is conveyed to the powders mixing chamber by Ar carrier gas. After homogenization, the powder mixture is injected through four channels embedded in the nozzle head into the melt pool. In each sample, at the end of each layer, to maintain the focal distance of the laser beam and the powder flow, the substrate is lowered to a pre-calculated level (based on our previous work [21]). By returning the nozzle to the starting point, the deposition process is repeated unidirectional for the subsequent layers. Fig. 2b shows a photograph of the samples fabricated according to the intended design (Fig. 2a) and under the constant processing parameters mentioned in Table 3. It should be noted that the beginning and end of each sample because the start and stop of powder injection occurred with a

Table 1 – Chemical composition of SS316 and IN718 powders (wt.%).

SS316L						
Fe	Cr	Ni	Mo	Mn	Si	C
Base	18	12	2	1.5	0.5	0.02
IN718						
Ni	Cr	Fe	Mo	Nb	Ti	Al
Base	18	10	2.5	5	1	1.2

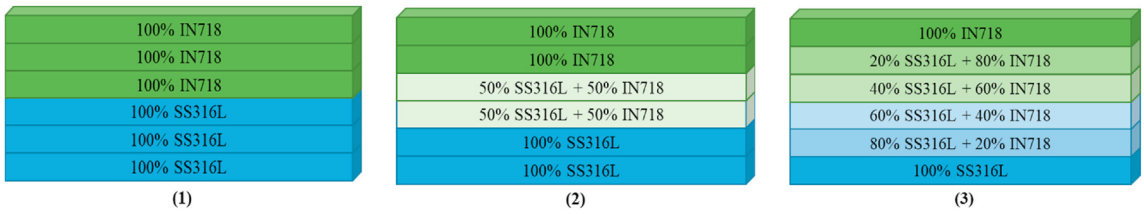

(a)

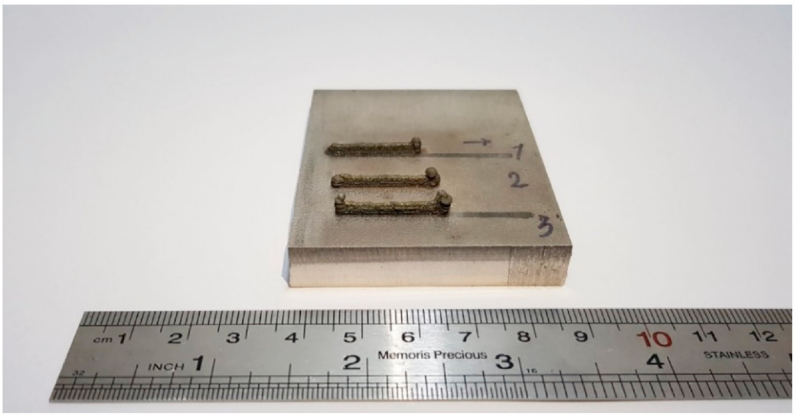

(b)

Fig. 2 – a) The design considered between the two alloys SS316L and IN718 and b) Additively manufactured samples (the arrow drawn on the substrate surface shows the direction of laser scanning).

slight delay compared to the laser beam, have a different appearance and unrelated to the rest of the sample length (in steady-state condition), and therefore these regions have been discarded in subsequent characterizations.

For experimental characterizations, the samples were cross-sectioned from the middle length using an electric discharge machine (EDM), and after mounting, their surface was prepared by standard metallographic techniques. Surfaces were also etched with 15 mL HCl + 5 mL HNO_3 solution for 10 s. An optical microscope (Olympus, Japan) and a scanning electron microscope (FEI ESEM QUANTA 200, USA) were used to evaluate the macrostructure and microstructure. Also, the X-ray energy dispersive spectroscope (EDAX EDS Silicon Drift 2017, USA) embedded in the SEM was used to investigate and measure the semi-quantitative distribution and segregation of constituent elements and the composition of detectable phases in the microstructure. In addition, Vickers microhardness (Buehler, Japan) was performed on the sections with a force of 300 grf and a dwell time of 10 s to measure hardness variations in the build direction (at intervals of every 260 μm). At each height of the structure, three microhardness measurements were performed to consider the measurement error, and the mean value was reported.

Table 2 – The adjusted rotation speed of the powder feeder discs for each layer of the samples.

Sample number	Layer number (composition)	Rotation speed of the powder feeder discs (rpm)	
		Feeder 1 (SS316L)	Feeder 2 (IN718)
1	1-3 (100% SS316L)	20	0
	4-6 (100% IN718)	0	29
2	1 & 2 (100% SS316L)	20	0
	3 & 4 (50% SS316L + 50% IN718)	9	16
	5 & 6 (100% IN718)	0	29
3	1 (100% SS316L)	20	0
	2 (80% SS316L + 20% IN718)	16	8
	3 (60% SS316L + 40% IN718)	12	14
	4 (40% SS316L + 60% IN718)	7	19
	5 (20% SS316L + 80% IN718)	3	24
	6 (100% IN718)	0	29

Table 3 – The fixed DLMD processing parameters used for the deposition.

Parameter	Value
Laser power (W)	250
Scanning speed (mm/min)	300
Axial gas flow (L/min)	3
Carrier gas flow (L/min)	1.5
Standoff distance (mm)	15
Z-increment between layers (mm)	0.8

3. Results and discussion

3.1. *Evaluation of macrostructure & microstructure*

Fig. 3 shows the cross-section macrostructure of the additive manufactured samples along with the design considered for each. The completely different reaction of the cross-section of sample 1 against the etching solution has made the areas of the two dissimilar alloys used in this sample's structure well recognizable, while due to the less differentiation of the corrosion resistance of adjacent layers in samples 2 and 3, the detection of chemical composition ranges is simply not possible. The close geometric characteristics of all three samples (determined on each) indicate appropriate reproducibility of the process, regardless of the type of structure design. Also, the layered structure, which is a feature of the AM process, is well recognizable in the macrographs. This effect is particularly pronounced in directed energy deposition (DED) techniques compared to powder bed fusion (PBF) because in the former, due to the use of higher input energy per unit length, the melt pool formed on the previous layer is puddle-shaped with a comparable length and depth (marked by the dashed line in Fig. 3a). This causes the direction of grain growth in DED techniques to have a significant deviation from the build direction, and curved columnar grains with a variety of orientations are formed along the structure because the direction of heat flow, in this case, is significantly affected by local positions at the melt pool boundary. However, in PBF techniques with long and shallow melt pool, the heat flow is often downward (almost independent of local positions at the melt pond boundary), and growth is in the build direction [19]. Another notable feature of the macrostructure is the porosities of various sizes in samples 2 and 3 (Fig. 3b and c). In fact, the absence of these defects in sample 1 and in contrast, the highest in sample 3 can be attributed to the use of powder mixtures, which due to the different thermal behavior of the base alloys, requires the use of specific processing parameters of that composition [15]; otherwise, thermal disorders will lead to such defects. This can be observed more in sample 3 than 2 because more powder mixtures with different proportions and various thermal behavior were used to fabricate the structure of sample 3.

By microscopy of the samples at a lower scale, the first phenomenon that attracts attention is changing the microstructure's morphology and size. As shown in Fig. 4, related to the optical microstructure along the cross-section (from top to bottom) of sample 1, the microstructure morphology alternates between cellular, columnar dendritic, and equiaxed growth. It is also noteworthy that the direction of cells/dendrites growth has a certain deviation from the build direction (<001>) because, as mentioned, the puddle-shaped of the melt pool during the process leads to change the direction of the maximum temperature gradient along the boundary of the melt pool and thus to change the direction of growth. On the other hand, it seems that the microstructure size varies along the cross-section, so that it can be said that it is the finest microstructure in the layers close to the substrate and the coarsest microstructure in the final layers. This suggestion can be expressed more confidently in SEM micrographs taken from different locations along the cross-section of sample 1 (compare Fig. 5a, b, and c).

The same phenomenon (change in morphology and size of the microstructure) is also observable for samples 2 and 3 (Fig. 6), with the difference that the morphology changes between adjacent layers in these two samples seems to be somewhat smoother with more epitaxial growth (as reported in Ref. [22]), which could be due to closer chemical composition of the adjacent layers. In general, the change in morphology and size of the microstructure of additive manufactured samples should be sought in solidification principles and concepts. Regarding the microstructure morphology resulting from solidification (regardless of modification techniques), the degree of stability of the solidification front (solid-liquid interface) determines the final morphology, which is dictated by the undercooling factor. The difference between equilibrium liquid temperature and local temperature in the solidification front is the total undercooling (ΔT_{tot}) which itself consists of other undercoolings as follows:

$$\Delta T_{tot} = \Delta T_C + \Delta T_T + \Delta T_K + \Delta T_R \quad (1)$$

where ΔT_C, ΔT_T, ΔT_K, and ΔT_R are undercoolings due to solute diffusion, thermal diffusion, kinetics, and curvature of the solid-liquid interface, respectively. Most engineering alloys, when solidified under usual conditions, ΔT_T, ΔT_K, and ΔT_R are small and negligible, and instead, the constitutional undercooling (ΔT_C) is predominant. The constitutional undercooling depends on several variables which based on them, the condition of stability of the solidification front can be parameterized as follows [23]:

$$\frac{G}{R} \quad \frac{m_L C_s^* (1 \quad k_0)}{k_0 D_L} \quad (2)$$

where G and R are the temperature gradient and solidification rate respectively, and m_L, C_s^*, k_0, and D_L are the liquidus line slope, the solid chemical composition at the interface, the distribution coefficient, and the liquid diffusivity, respectively. Accordingly, in the additive manufactured samples, the degree of solidification front instability should be increased from the initial layers to the final layers, and as a result, the microstructure should continuously evolve from cellular to columnar dendritic and from columnar dendritic to equiaxed dendritic. This is expected because as the process progresses and the deposition height increases, due to the reduction of heat dissipation through thermal conduction and as a result of heat accumulation, the temperature gradient (G) decreases and therefore, according to inequality (2), the stability of the solidification front becomes more difficult. In addition,

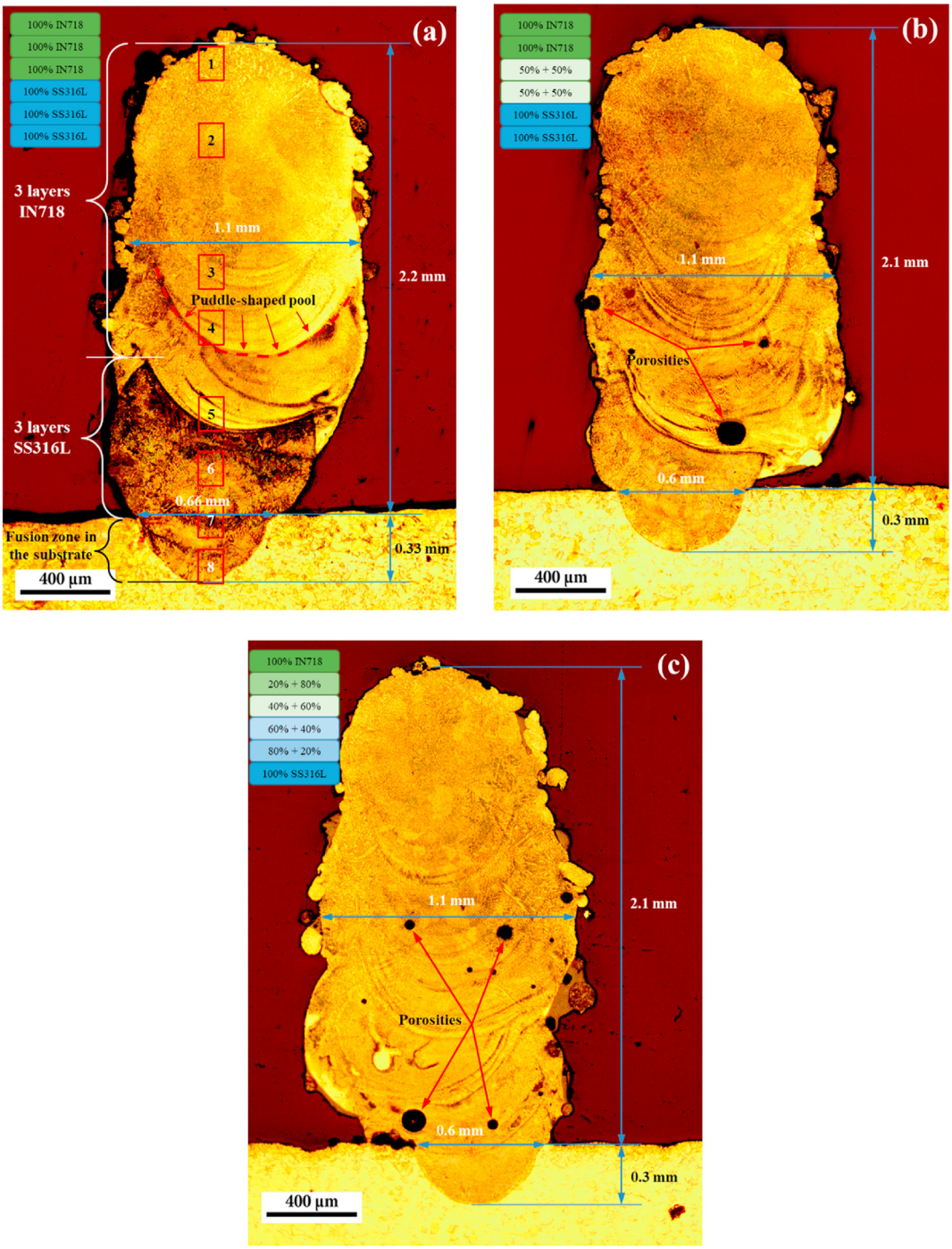

Fig. 3 – The Macrostructure and geometric characteristics of the cross-section of samples a) 1, b) 2, and c) 3, next to the relevant design. The numbered boxes in (a) were selected for the optical microstructure evaluation.

although more accurate thermodynamic calculations are needed, it can be said that by changing the feed container to powder rich in various alloying elements of IN718 (sample 1) or adding it to the feeding powder composition (samples 2 and 3), on the right side of inequality (2), the chemical composition variable (C_s^*) increases, and due to the addition of elements with a lower distribution coefficient (such as niobium and molybdenum) to the powder mixture, the distribution coefficient (k_0) also decreases, both of which lead to a decrease in the stability of the solidification front according to the inequality. However, microscopic investigations have shown that the evolution of microstructure in the samples is not continuous, and the morphology sometimes varies periodically between solidification modes (cellular, columnar dendritic, and equiaxed dendritic). This is due to the fact that AM is not essentially a continuous process. Each layer, in addition to the initial solidification during its creation, also experiences melting and solidification again with the deposition of the

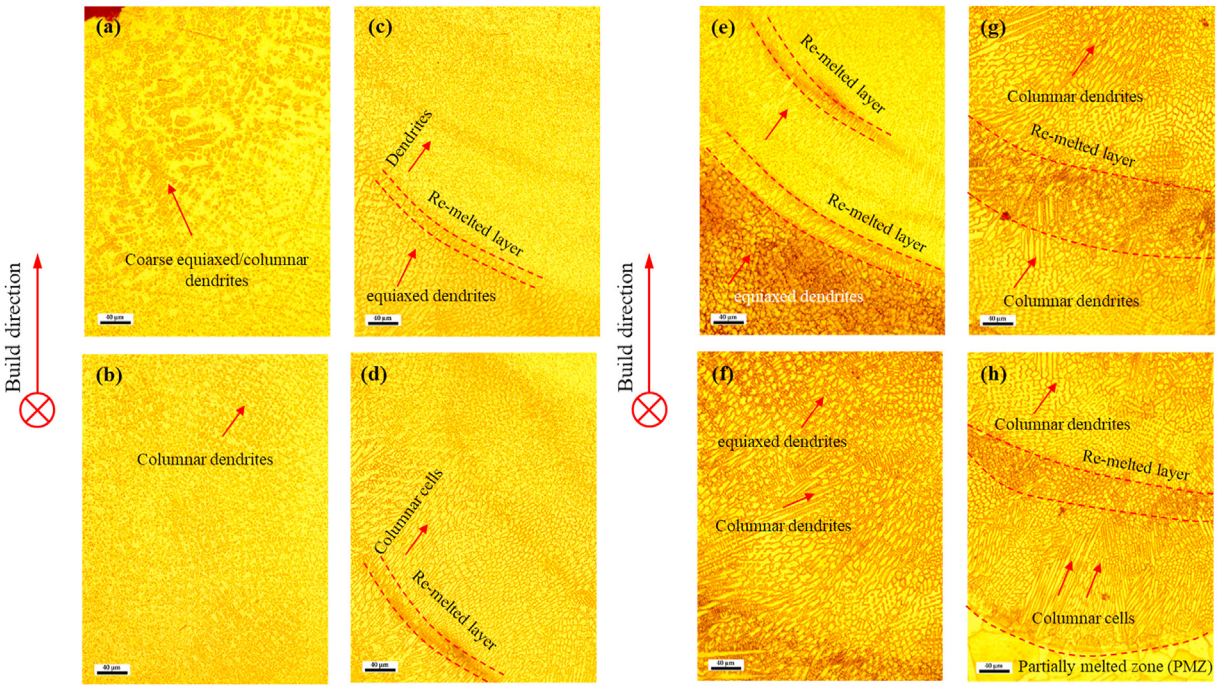

Fig. 4 – Evolution of microstructure along the cross-section of sample 1, from a) box num. 1 to h) box num. 8 in Fig. 3a (from the outermost layer to the innermost).

subsequent layer (enclosed areas between the dashed lines in Figs. 4–6), the extent of which depends on factors such as the input energy density and the delay time between two adjacent layers.

Regarding the microstructure size, in general, the determining factor is the cooling rate (*CR*), which is related to the dendritic arms spacing (λ, an indicator of the microstructure size) as follows [24]:

$$\lambda = b(CR)^{n} \tag{3}$$

where b and n are the constants of the material. As can be physically understood, Eq. (3) states that as the cooling rate

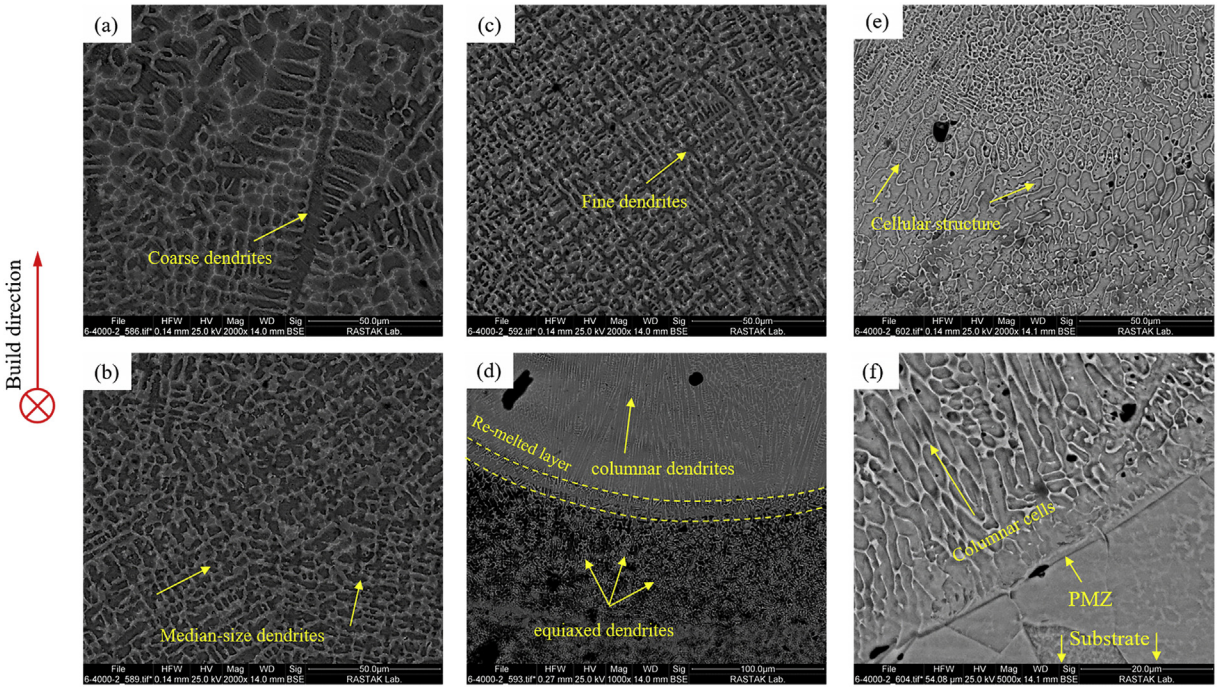

Fig. 5 – The SEM micrographs along the cross-section of sample 1, from the outermost layer in (a) to the innermost in (f).

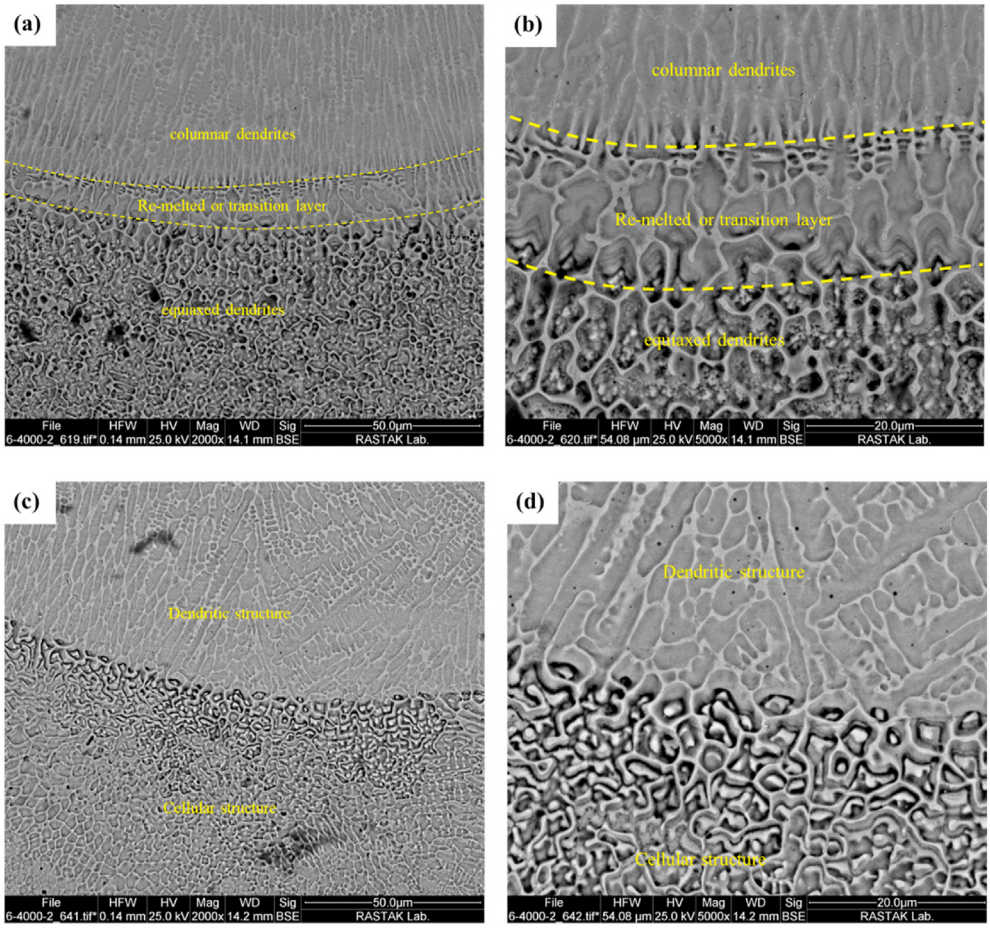

Fig. 6 – The microstructure morphology at the interface of two adjacent layers in samples a, b) 2 and c, d) 3. (b) and (d) are larger magnifications of (a) and (c), respectively.

decreases, the space between the dendritic arms increases, resulting in a coarser microstructure. Although due to the discontinuity of the process, exceptions can be observed in describing the change in microstructure size in the build direction (especially at the bottom and top of each layer), but regardless of them, generally with increasing deposition height, the temperature gradient decreases due to the heat accumulation, and according to Eq. (4), the cooling rate also decreases, which has increased the microstructure size along the build direction, so that the coarsest size is related to the microstructure of the outermost layer and the finest is related to the innermost layer.

$$CR : \frac{dT}{dt} = \frac{dT}{dx}.\frac{dx}{dt} \rightarrow CR = G.R \tag{4}$$

In Eq. (4), T, t, and x are temperature, time, and distance, respectively.

3.2. *Evaluation of chemical & phase composition*

In order to investigate the effect of the transition designs between the base alloys on chemical distribution, EDS line analysis was performed along the cross-section of the samples which the analysis path and its results for the three samples are shown in Fig. 7. It is noteworthy that due to the concentration of elements in the base alloys, for better detection, semi-quantitative and comparative measurements of the main elements Fe, Ni, and Cr were found to be sufficient. In sample 1, although the design and fabrication were done in the form of a direct transition between SS316L and IN718, the formation of an intermixing zone at the interface between the two alloys about 200 μm wide (Fig. 7a) illustrates another fact. Actually, the formation of such a zone, which leads to a kind of gradation of the direct transition and has been mentioned in some studies [15,16], is due to the dilution between adjacent layers, which in the case of sample 1 due to the significant difference between the chemical composition (especially the two elements Fe and Ni) of the two intermediate layers, it is well detectable by the chemical analysis. Furthermore, comparing the results in Fig. 7b–d shows that by changing the sample design from 1 to 2 and from 2 to 3, as expected, the transition between the base alloys has been more gradual. On the one hand, this shows the ability of the additive manufacturing process to produce gradient materials; on the other hand, it indicates a good potential to improve the performance and service life of parts made of

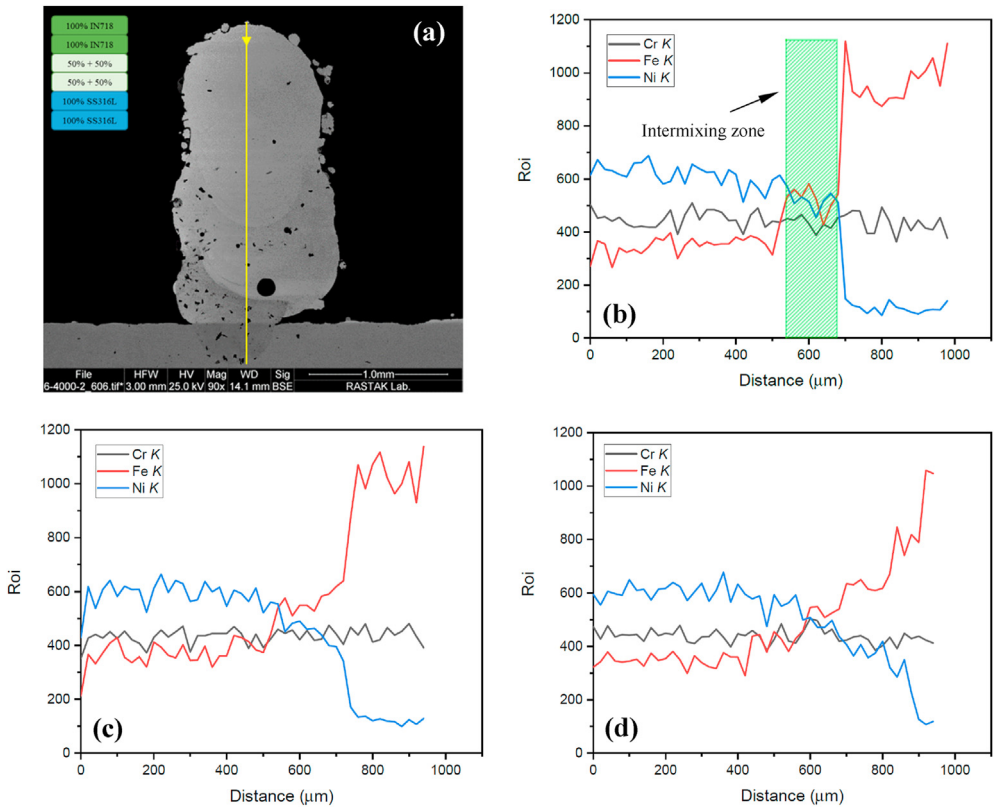

Fig. 7 – a) The Macrograph of the cross-section of sample 2 and the path specified on it for the EDS line analysis. b–d) The chemical analysis results along the cross-sections similar to (a) for samples 1, 2, and 3, respectively.

dissimilar materials through smooth change between the properties and behavior of adjacent layers.

Another aspect that attracts attention when evaluating microstructure along cross-sections is the significant contrast of inter-dendritic/cellular spaces, which indicates a different

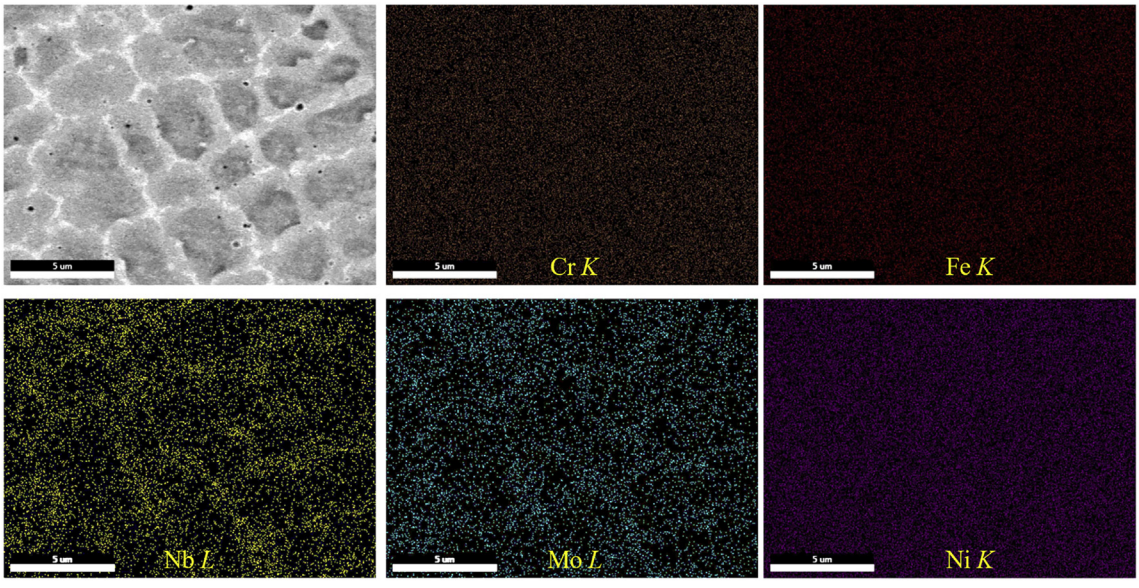

Fig. 8 – The Microstructure morphology and distribution maps of relevant elements from the outermost layer in sample 1.

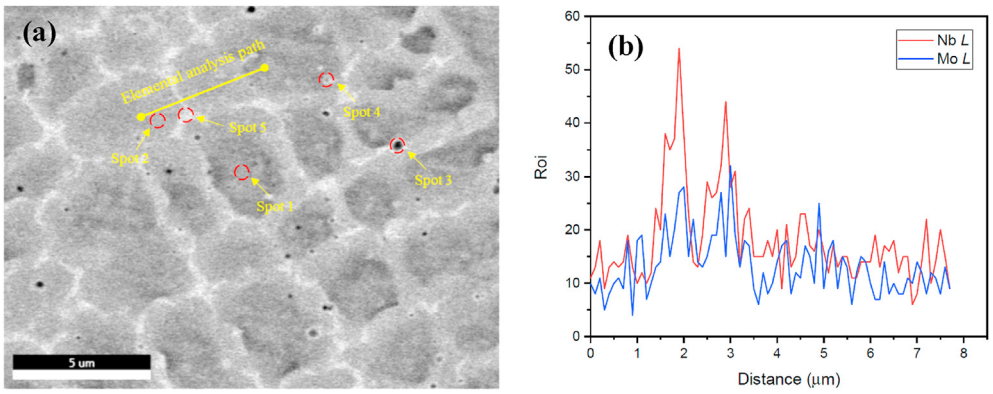

Fig. 9 – The microstructure morphology of the outermost layer in sample 1, with the path and points designated on it for elemental analysis by EDS. b) Distribution of Nb and Mo elements along the path specified in (a).

composition from dendrites/cells core. Regardless of the typical structure of austenite and inter-dendritic/cellular delta ferrite (δ) in solidification of SS316L rich layers (Fig. 4e–h), this issue especially exists in layers with a high percentage of IN718 alloy. Fig. 8 shows the microstructure morphology and element distribution maps associated with the outermost layer in sample 1. As the element distribution maps show, the two elements Nb and Mo have a more noticeable presence in the interdendritic spaces, while for the three main elements Ni, Fe, and Cr, no obvious distinction can be seen throughout the presented microstructure. In addition, according to Fig. 9a, b, the Nb and Mo microsegregation in the EDS line analysis for the distance between two adjacent dendritic arms are well understood. In fact, during solidification with the growth of gamma (γ) dendrites as the initial phase (gray areas in Fig. 9a), elements with low distribution coefficients (e.g., Nb, Ti, C, and Mo) are rejected into the interdendritic melt, and as the melt is enriched with these elements, secondary phases begin to form. In the presence of IN718 superalloy, the formation of MC carbides (such as NbC) is one of the possible types of secondary phases that, with their formation (dark particles in Fig. 9a), the interdendritic melt is depleted of carbon and while still rich in other alloying elements, the formation of the Laves phase occurs through the eutectic reaction $L \rightarrow \gamma + \text{Laves}$ (white areas in Fig. 9a). An interesting point that can be mentioned is the presence of the Laves phase around or in contact with carbide particles, which has been observed in other studies related to the additive manufacturing of IN718 [25,26]. It is noteworthy that Radhakrishnan and Thompson [27] had previously proposed two different morphologies of the three-phase mixture and divorced eutectic for the Laves/NbC/γ ternary eutectic. In general, the formation of Laves intermetallic phase with hexagonal structure and general chemical formula $(Ni, Cr, Fe)_2(Nb, Mo, Ti)$ due to the depletion of the γ matrix of alloying elements and its brittle nature has a detrimental effect on mechanical properties [26,28]. Also, due to its low melting point and often its continuity at the grain/dendrite boundaries, it has encouraged the nucleation and propagation of liquation cracks along additive manufactured structures [29]. Fig. 10 shows the EDS chemical analysis results of the points shown in Fig. 9a, which supports the discussions about the microstructure's phase composition.

3.3. *Evaluation of microhardness*

Fig. 11a shows the microhardness variations along the cross-section of the samples according to the design on the macrostructure of sample 1 in Fig. 11b (from all three measurements at a same height, the mean value was reported). In sample 1, as can be seen, the hardness first increases and then decreases abruptly. The initial increase in hardness to the third position in sample 1 may be caused by slight development of the delta ferrite phase (δ) due to the facilitation of solute elements redistribution by decreasing the cooling rate due to thermal accumulation during the process [30]. More corrosion traces (darker) in the third position of the microhardness measurement compared to the first position on the optical macrostructure of sample 1 (Fig. 11b) due to a different reaction with the etching solution can be a reason for increasing the δ phase fraction (with weaker corrosion resistance than austenite) to the third position of hardness. After that, due to the evolution of the soft phase of austenite (as the matrix phase) by the deposition of IN718 nickel-based superalloy, the hardness is significantly reduced. However, this decrease in hardness from sample 1 to 2 and from 2 to 3 more smoothly occurred due to the gradation of the dissimilar structure of SS316L-IN718 and as a result of closer properties and behavior of adjacent layers. As in sample 3, considering the deviation from the mean, hardness variation along the structure is very small, and hardness values are close to each other. This achievement (proximity of properties and behavior of adjacent layers in dissimilar structures) can significantly affect the improving service life and preventing premature failure of parts [2]. It should be noted that no re-increase of

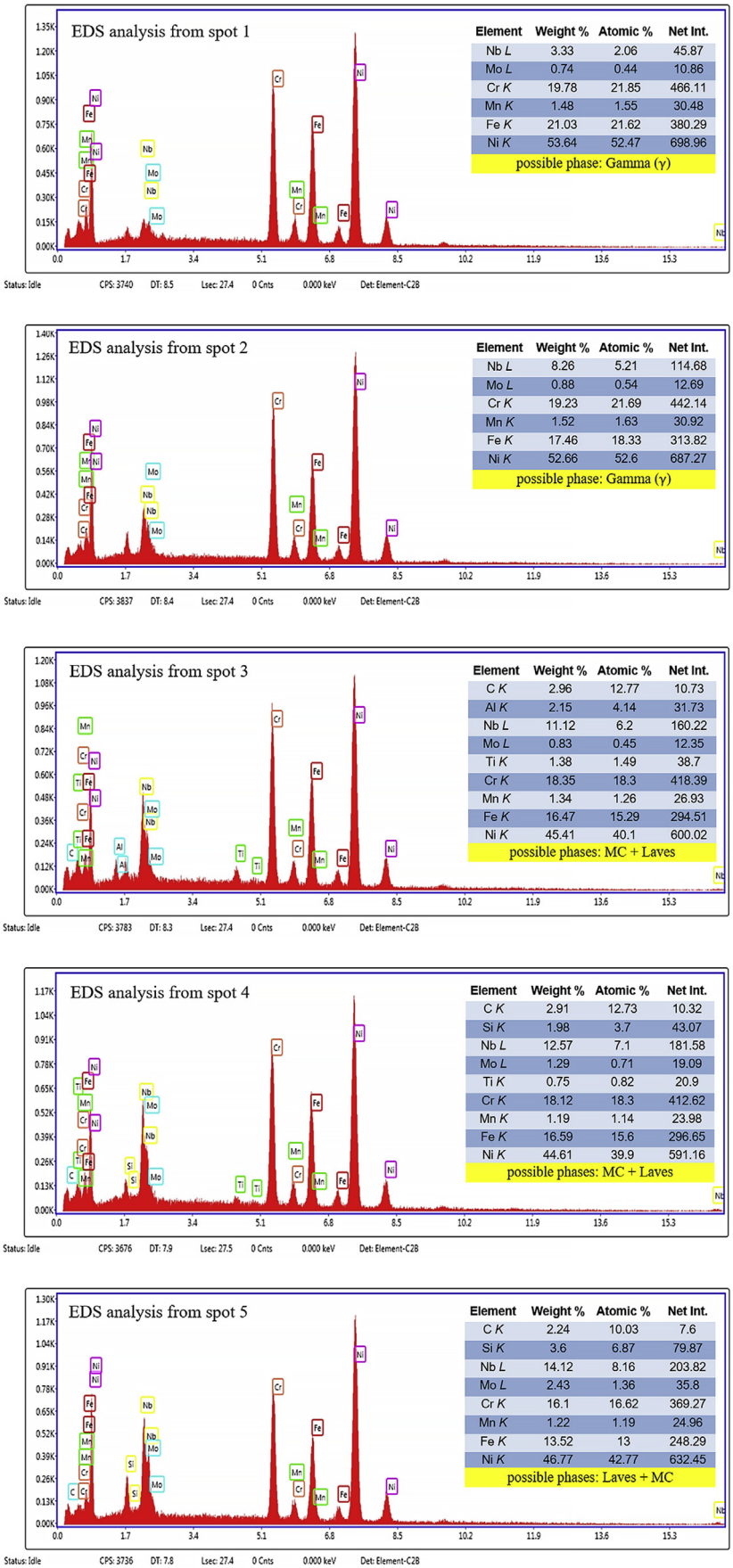

Fig. 10 – The Chemical analysis results of the points shown in Fig. 9a, along with the phase predictions for each.

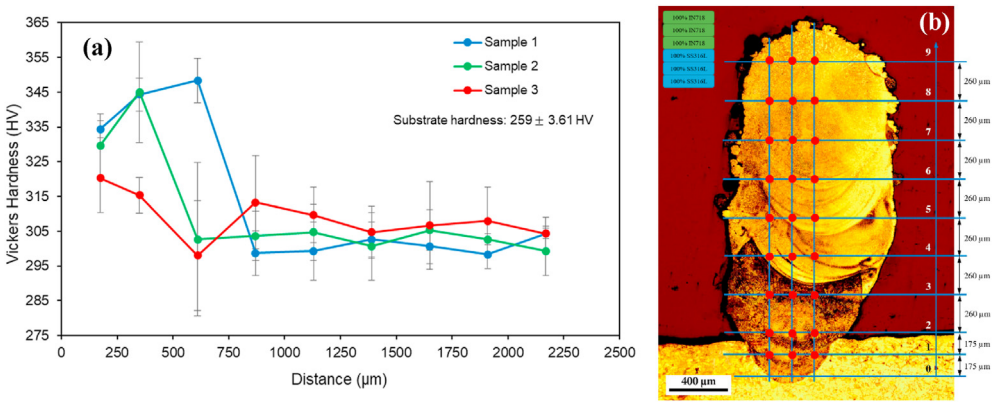

Fig. 11 – a) Microhardness variations along the cross-section of samples 1, 2, and 3 according to b) the design considered on the macrostructure of sample 1 (all three measurements at the same height were calculated and reported as the mean value).

hardness due to the carbide and intermetallic (Laves) phases, which have been reported in Refs. [14,18], could be due to their limited evolution and small size compared to austenite dendrites as matrix phase. In other words, the high cooling rate and low reheating cycles)by only six layers deposition in all three samples (lead to the lack of time and activation energy required for diffusion-dependent phase transformations, resulting in non-equilibrium and supersaturated microstructures. Thus, in the final layers of the studied structures, the hardness has not increased again due to the low fraction of the secondary phases.

4. Conclusion

In the present study, additive manufacturing of the thin-walled dissimilar structure of SS316L-IN718 with three different transition designs by direct laser metal deposition (DLMD), in terms of macrostructure, microstructure, chemical distribution, phase evolution, and microhardness variations in the build direction was evaluated that the most important results are as follows:

1) In macrostructural evaluations, it was found that by changing the transition design from direct (sample 1) to gradient (samples 2 and 3), several porosities appear along the structure, indicating thermal disorders and the need to use specific processing parameters of that composition.
2) Microstructural evaluations showed that although due to the undercooling increase in the build direction, there is a tendency for the continuous evolution of solidification morphology in this direction as cellular → columnar dendritic → equiaxed dendritic, sometimes the periodic repetition of solidification morphologies can be seen due to the discontinuity of the AM process and therefore re-melting and solidification of layers. Also, in general, with increasing deposition height, due to the decrease in cooling rate caused by thermal accumulation, a coarser microstructure is formed in the final layers.
3) Chemical evaluation along the cross-section of the samples showed that in addition to the more gradual distribution of elements in the dissimilar thin-walled structures with gradient layers (samples 2 and 3) as expected, in the direct transition (sample 1), an intermixing zone is formed at the interface between the two alloys, due to the dilution between adjacent layers, which causes it to a kind of gradient. In addition, microsegregation of elements with low distribution coefficients in the intercellular/dendritic regions during the non-equilibrium solidification of the process (especially with increasing IN718 participation in the deposition) led to the formation of secondary phases such as MC carbide and Laves intermetallic compound.
4) Comparison of microhardness variations along the cross-section of the three samples with different transition designs between the base alloys showed that the gradation of the dissimilar structure minimizes the sudden changes due to the closer properties and behavior of adjacent layers, which can be very useful in improving the service life and preventing premature failure of parts.

Declaration of Competing Interest

The authors declare that they have no known competing financial interests or personal relationships that could have appeared to influence the work reported in this paper.

Acknowledgments

The authors would like to acknowledge the financial support for this research from Iran National Science Foundation (Grant No. 99011515).

REFERENCES

[1] Bhavar V, Kattire P, Thakare S, Singh RK. A review on functionally gradient materials (FGMs) and their

applications. In: IOP Conference Series: Materials Science and Engineering. IOP Publishing; 2017.
[2] Ghanavati R, Naffakh-Moosavy H. Additive Manufacturing of Functionally Graded Metallic Materials: A Review of Experimental and Numerical Studies. J Mater Res Technol 2021;13:1628–64.
[3] Mahamood RM, Akinlabi ET. Functionally Graded Materials. Springer International Publishing; 2017.
[4] Naebe M, Shirvanimoghaddam K. Functionally graded materials: A review of fabrication and properties. Appl Mater Today 2016;5:223–45.
[5] Mahamood RM, Akinlabi ET, Shukla M, Pityana SL. Functionally graded material: an overview. In: Proceedings of the World Congress on Engineering. WCE; 2012.
[6] Hofmann DC, Kolodziejska J, Roberts S, Otis R, Dillon RP, Suh JO, et al. Compositionally graded metals: A new frontier of additive manufacturing. J Mater Res 2014;29(17):1899–910.
[7] Zhang C, Chen F, Huang Z, Jia M, Chen G, Ye Y, et al. Additive manufacturing of functionally graded materials: A review. Mater Sci Eng: A 2019;764:138209.
[8] DebRoy T, Mukherjee T, Milewski JO, Elmer JW, Ribic B, Blecher JJ, et al. Scientific, technological and economic issues in metal printing and their solutions. Nat Mater 2019:1.
[9] Yan L, Chen Y, Liou F. Additive manufacturing of functionally graded metallic materials using laser metal deposition. Addit Manuf 2020;31:100901.
[10] Reichardt A, Shapiro AA, Otis R, Dillon RP, Borgonia JP, McEnerney BW, et al. Advances in additive manufacturing of metal-based functionally graded materials. Int Mater Rev 2020:1–29.
[11] Rodriguez J, Hoefer K, Haelsig A, Mayr P. Functionally graded SS 316L to Ni-based structures produced by 3D plasma metal deposition. Metals 2019;9(6):620.
[12] Robinson JL, Scott MH. Liquation cracking during the welding of austenitic stainless steels and nickel alloys. Phil Trans Roy Soc Lond Ser A Math Phys Sci 1980;295(1413):105–17.
[13] Lin X, Yue TM, Yang HO, Huang WD. Laser rapid forming of SS316L/Rene88DT graded material. Mater Sci Eng: A 2005;391(1-2):325–36.
[14] Shah K, ul Haq I, Khan A, Shah SA, Khan M, Pinkerton AJ. Parametric study of development of Inconel-steel functionally graded materials by laser direct metal deposition. Mater Des 2014;54:531–8.
[15] Savitha U, Reddy GJ, Venkataramana A, Rao AS, Gokhale AA, Sundararaman M. Chemical analysis, structure and mechanical properties of discrete and compositionally graded SS316–IN625 dual materials. Mater Sci Eng: A 2015;647:344–52.
[16] Zhang X, Chen Y, Liou F. Fabrication of SS316L-IN625 functionally graded materials by powder-fed directed energy deposition. Sci Technol Weld Join 2019;24(5):504–16.
[17] Carroll BE, Otis RA, Borgonia JP, Suh JO, Dillon RP, Shapiro AA, et al. Functionally graded material of 304L stainless steel and inconel 625 fabricated by directed energy deposition: Characterization and thermodynamic modeling. Acta Mater 2016;108:46–54.
[18] Su Y, Chen B, Tan C, Song X, Feng J. Influence of composition gradient variation on the microstructure and mechanical properties of 316 L/Inconel718 functionally graded material fabricated by laser additive manufacturing. J Mater Process Technol 2020;283:116702.
[19] DebRoy T, Wei HL, Zuback JS, Mukherjee T, Elmer JW, Milewski JO, et al. Additive manufacturing of metallic components–process, structure and properties. Prog Mater Sci 2018;92:112–224.
[20] Oliveira JP, Santos TG, Miranda RM. Revisiting fundamental welding concepts to improve additive manufacturing: From theory to practice. Prog Mater Sci 2020;107:100590.
[21] Moradi M, Ashoori A, Hasani A. Additive manufacturing of stellite 6 superalloy by direct laser metal deposition–Part 1: Effects of laser power and focal plane position. Opt Laser Technol 2020;131:106328.
[22] Chen N, Khan HA, Wan Z, Lippert J, Sun H, Shang SL, et al. Microstructural characteristics and crack formation in additively manufactured bimetal material of 316L stainless steel and Inconel 625. Addit Manuf 2020;32:101037.
[23] Flemings MC. Solidification processing. Materials Science and Technology; 2006.
[24] Kou S. Welding metallurgy. 2 ed. New Jersey, USA: John Wiley & Sons; 2003.
[25] Parimi LL, Ravi GA, Clark D, Attallah MM. Microstructural and texture development in direct laser fabricated IN718. Mater Char 2014;89:102–11.
[26] Ding RG, Huang ZW, Li HY, Mitchell I, Baxter G, Bowen P. Electron microscopy study of direct laser deposited IN718. Mater Char 2015;106:324–37.
[27] Radhakrishnan B, Thompson RG. Solidification of the nickel-base superalloy 718: a phase diagram approach. Metall Trans A 1989;20(12):2866–8.
[28] Chen B, Su Y, Xie Z, Tan C, Feng J. Development and characterization of 316L/Inconel625 functionally graded material fabricated by laser direct metal deposition. Opt Laser Technol 2020;123:105916.
[29] Chen Y, Zhang K, Huang J, Hosseini SR, Li Z. Characterization of heat affected zone liquation cracking in laser additive manufacturing of Inconel 718. Mater Des 2016;90:586–94.
[30] Zhang CH, Zhang H, Wu CL, Zhang S, Sun ZL, Dong SY. Multi-layer functional graded stainless steel fabricated by laser melting deposition. Vacuum 2017;141:181–7.